Journal of Molecular Liquids 348 (2022) 118206

Contents lists available at ScienceDirect

Journal of Molecular Liquids

journal homepage: www.elsevier.com/locate/molliq

Lubricant-enhanced self-transport of condensed nanodroplets trapped in Wenzel state

Lin Guo [a], Wenqing Shen [b], Kumar Satish [b], Zhigang Liu [a,*], Guihua Tang [c,*]

[a] Energy Research Institute, Qilu University of Technology, Jinan 250014, PR China
[b] G. W. Woodruff School of Mechanical Engineering, Georgia Institute of Technology, Atlanta GA 30332, USA
[c] MOE Key Laboratory of Thermo-Fluid Science and Engineering, School of Energy and Power Engineering, Xi'an Jiaotong University, Xi'an 710049, PR China

ARTICLE INFO

Article history:
Received 8 August 2021
Revised 27 September 2021
Accepted 23 November 2021
Available online 10 December 2021

Keywords:
Droplet
Self-driven
Condensation
Molecular dynamics simulation

ABSTRACT

Condensates are extremely easy to be trapped in micro/nano-gaps of surfaces and stay in the sticky Wenzel wetting state due to the nucleation. Rather than avoiding the unexpected Wenzel state, an efficient detachment of Wenzel condensates is targeted in present work. A bionic lubricant-impregnated wedge-groove surface is proposed inspired by a combination of the conical cactus spines and the oil-immersion structure of pitcher plants. The dynamic behaviours of a single nanodroplet and condensates are investigated using molecular dynamics simulations. By taking advantage of the conical structure and the thoroughly wetted liquid–solid interface in the groove, droplets trapped in the Wenzel state are observed to move spontaneously on the proposed patterned surface, while droplets in the Cassie state are found immobile. Moreover, the nucleation sites can be controlled and the nucleation energy barriers are also reduced by the proposed surface. The present work can pave a new path to manipulate the droplets in the sticky Wenzel state with higher nucleation and drainage rate, which is desired to provide an energy-efficient method for efficient condensation.

1. Introduction

Vapour condensation is widely applied and of large potential in many situations, including electronic cooling, desalination, and fog-harvesting [1–6]. Dropwise condensation is preferred than filmwise condensation, due to its high efficiency in heat transfer [7]. Moreover, the wetting of initially-formed nanodroplets has significant effects on the growth, coalescence and sliding of microdroplets [8,9]. So how to enhance the sliding of condensing nanodroplets is a critical question, compared with the stable sessile microdroplets.

In dropwise condensation, as we know, wetting in slippery Cassie mode can present a small sliding angle due to underlying air pockets at liquid–solid interfaces [10] on certain functional micro/nano-structured surfaces [11–13], while it is easy for condensing droplets to be trapped in micro/nano-gaps, leading to a sticky Wenzel wetting state [14,15]. Hierarchical structured surfaces are developed for this issue. For instance, nanowires with a high height-to-diameter ratio are usually adopted to avoid the unexpected Wenzel state [16] or to guide the existing Wenzel condensates to transit to the Cassie state [17–19]. Then the condensates can be removed by gravity or coalescence-induced jumping [20–23]. Actually, a huge of efforts have been devoted to how to avoid unexpected Wenzel state, although these efforts may suffer from problems like the narrow range of subcooling degree or secondary flooding [24,25].

Here, the present work would like to turn to a different direction for possible solution. In the community of micro/nano fluids, directional self-propulsion of droplets is extensively investigated due to its high energy efficiency compared with external forces-based methods [26]. In addition, this idea may not require a Cassie mode wetting, and actually it encourages to take advantage of the sticky Wenzel state to drive droplets [27,28]. The manipulation of Wenzel condensates can also improve the surface stability as well as the applicable subcooling degree [29,30].

However, even though the self-transportation of Wenzel droplets remains a significant challenge, many advances have been obtained under the inspiration of nature world [31]. Similarly, micro/nano-structures is also employed for an optimization of the solid–liquid interfacial tension [32]. For example, Ju et al. found that the conical structure of cactus spines can make the droplet move spontaneously from the tip to the base of the spine under the combined action of Laplace pressure difference and wetting gradient difference [33,34]. Wong et al. analyzed the oil-

* Corresponding authors.
E-mail addresses: zgliu9322@163.com (Z. Liu), ghtang@mail.xjtu.edu.cn (G. Tang).

https://doi.org/10.1016/j.molliq.2021.118206
0167-7322/

immersion interface of pitcher plants [35]. The water–solid interface is changed to water-lubricant-solid interface by the lubricant, so the friction force is greatly reduced and the droplets can slide rapidly [36].

Except for pure nanostructures, lubricant is paving a new path to adjust the droplet interfacial dynamics. For example, it is found in our previous work [37] that a droplet on a lubricant-impregnated surface can present three type of interfaces and their combinations of eight types [38]. In that work, Molecular Dynamics (MD) method [37] successfully captures the complex morphology of droplets in a multi-phase system of water, lubricant and solid. When we revisit the previous results, we realize that a type of wetting state, where the droplet is not clocked by the lubricant but encapsulated on the lubricant-impregnated surface, can be of great potential for the present problem, to drive condensing nanodroplets for condensation enhancement.

Coincidentally, the authors ever carried experimental work on both the above two topics. In 2015, Guo and Tang carried experimental and theoretical investigation on the self-driven process of a single droplet on cactus spines, presenting a speed of as high as 1.17 m/s, and exhibiting the high efficiency of self-propulsion [34]. In 2018, they prepared a copper-based hydrophilic-slippery surface by depositing a lubricant onto the micro-structured copper substrate and obtained an efficient dropwise condensation on hydrophilic surface [39]. Thus, inspired by both the conical cactus spines and the oil-immersion structured surface, a bionic lubricant-impregnated wedge-groove surface is proposed in the present work.

We are aiming to examine a novel concept of surface design, where the droplet can be in a slippery Wenzel state if sinking into the gaps of micro/nano-structures, whose sliding angle is extremely small [40]. Water molecules will nucleate at the liquid-lubricant interface and grow and merge during condensation [41]. Thus, it is possible for the condensates to move spontaneously and efficiently due to the lubricant-impregnated wedge-groove structures. Prior to dynamics of condensing droplets, the behaviours of existing droplets are firstly investigated. The dependence of their self-propulsion on surface conditions is explored, including the wetting state, lubricant thickness, cone angle, and groove depth. Then, the coupling of condensation and self-propulsion is examined on five types of solid surfaces for comparisons.

2. Methodology

2.1. MD modelling basics

To explore the self-driven transport on the proposed lubricant-impregnated wedge-groove surface (Wedge-groove LIS), the MD simulation is performed using the LAMMPS platform. The patterned surfaces, shown in Fig. 1, are constructed with platinum (Pt) atoms. To reduce the computational cost and extend the time and length scales compared to the all-atom model, we apply a coarse-grained model for water molecules where four water molecules are represented by one coarse-grained bead (W). The hexane-like structure has been validated to be able to predict the morphologies and dynamic characters of the lubricant-impregnated surface in our previous studies [37,41]. Concretely, hexane is considered as the lubricant with two coarse-grained particles (CT-CT) represent one hexane molecule and each particle (CT) contains three CH_2/CH_3 groups. The bond type of hexane particles is harmonic with the coefficient of 5.9725 kcal·mol^{-1} Å^{-2}, and the bond length of 3.6 Å.

Morse potential is used for particle–particle interactions of water (W-W) and hexane (CT-CT), which has the form

$$E_{\mathrm{W-W,CT-CT}} = D_0\left[e^{-2\alpha(r-r_0)} - 2e^{-2\alpha(r-r_0)}\right], r < r_c, \quad (1)$$

where r_c is the cutoff.

The standard 12/6 Lennard-Jones potential is used for the interaction of platinum/platinum (Pt-Pt), water/platinum (W-Pt), and hexane/platinum (CT-Pt), which can be given by

$$E_{\mathrm{Pt-Pt,W-Pt,CT-Pt}} = 4\varepsilon\left[\left(\frac{\sigma}{r}\right)^{12} - \left(\frac{\sigma}{r}\right)^{6}\right], r < r_c, \quad (2)$$

where σ is calculated from the arithmetic average between the particles following Lorentz-Berthelot mixing rules. Different wettabilities for water and hexane can be obtained by changing ε.

The Lennard-Jones potential 12/4 LJ is used for the water and hexane interactions (W-CT), given by

$$E_{\mathrm{W-CT}} = \frac{3\sqrt{3}}{2}\varepsilon\left[\left(\frac{\sigma}{r}\right)^{12} - \left(\frac{\sigma}{r}\right)^{6}\right], r < r_c, \quad (3)$$

where σ is calculated from the arithmetic average between the particles. ε can be obtained based on interfacial tensions between water and hexane. The verification and more details of the present computational model can be found in Ref. [41]. Pair styles and pair coefficients applied in the present work are listed in Table. 1.

2.2. Nano-structured surface

Parallel-groove refers to the surface with a groove that is parallel while wedge-groove refers to the surface with a groove in wedge shape, see Fig. 1a. Wedge-groove LIS refers to the wedge-groove surface with lubricant impregnated. Its construction contains two steps, as shown in Fig. 2a. Step 1: the wedge-groove structure is built as the substrate; Step 2: the hexane beads are placed on the top of the substrate; Step 3: the whole system is equilibrated at 300 K using a Nose/Hoover thermostat with a time step of 10 fs for 1 ns. The hexane beads will fully wet and form a film on the surface, thus the lubricant-impregnated state is obtained. The geometry is controlled by the following four parameters: the groove length L, the conical angle α, the spacing s when $y = L$, and the groove depth h. The hexane number applied in this section is 2244. In this case, the hexane can completely wet and form a thin layer on the solid substrate. Therefore, considering effects of the lubricant thickness, the spacing and the groove depth of the wedge-groove LIS are set to be slightly larger than the wedge-groove surface. Surface geometrical parameters are shown in Fig. 1b and listed in Table. 2.

2.3. Sessile droplets on patterned surfaces

For a static droplet on patterned surfaces, a water droplet containing 4200 water beads is built and placed on the constructed patterned surface with the y-coordinate of the center of L, as shown in Fig. 2a. The computational box size is 156.8 × 274.4 × 2 50.8 Å^3, and the periodic boundary condition is applied to all the three directions. The y-coordinate of the nanodroplet is fixed and the whole system is equilibrated at 300 K using a Nose/Hoover thermostat with a time step of 10 fs for 1 ns. Snapshots of the droplet morphologies are collected and the static states are obtained. After the simulation of the static state of the single nanodroplet, the y-coordinate of the droplet is unfixed. The entire system is equilibrated in an NVE ensemble for 10 ns with a time step of 10 fs, shown as Step 4 in Fig. 2a. The droplet movement is tracked every 0.1 ns and the average velocity is calculated.

2.4. Vapor condensation modelling

The condensation system is built and shown in Fig. 2b, with the settings of simulation configuration. The liquid film at the top of the simulation box is used as a vapor source, and the solid surface

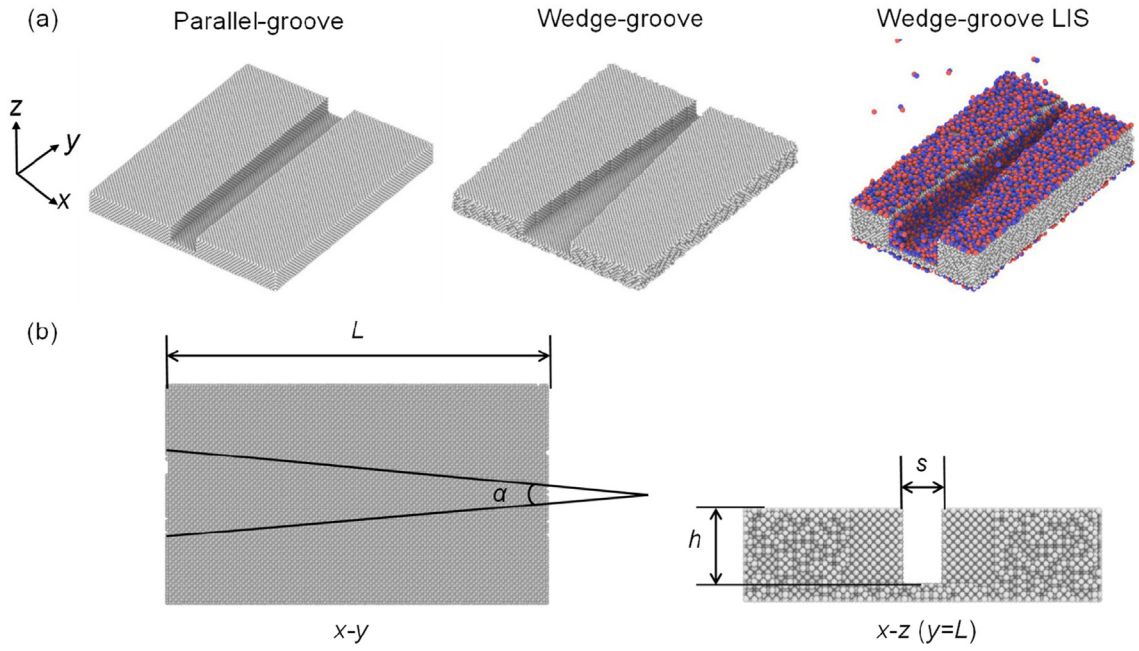

Fig. 1. Geometry structures. (a) Illustration of the patterned surfaces. Parallel-groove refers to surface with groove that is parallel; Wedge-groove refers to surface with groove that is in wedge shape; Wedge-groove LIS refers to wedge-groove surface with lubricant impregnated. (b) Geometrical parameters presented in the *x-y* section and *x-z* section. *L* refers to the groove length, α refers to the conical angle of the groove, *s* refers to the spacing when $y = L$, and *h* refers to the groove depth.

Table 1
Parameter settings of molecular potential functions.

Interaction site	Pair style	Pair coefficients			
		D_0 / eV	α /Å^{-1}	r_0 / Å	r_c /Å
W-W	Morse	0.0351	0.556	6.29	16
CT-CT	Morse	0.0304	1.139	5.27	16
		ε / eV	σ / Å	r_c / Å	
Pt-Pt	12/6 LJ	0.6969	2.471	13	
W-Pt	12/6 LJ		3.586	13	
CT-Pt	12/6 LJ	0.02	3.528	13	
		ε / eV	σ / Å	r_c / Å	
W-CT	12/4 LJ	0.0152	4.642	15	

on top of this film is treated as the heat source (Pt_{up}). The solid surface on the bottom of the simulation box is treated as the surface for condensation (Pt_{down}) with lubricant on top of it. There are two steps of the simulation procedure. The hexane-Pt_{down} system and the water-Pt_{up} system are firstly separately equilibrated in an NVT ensemble at 300 K and 550 K with a time step of 10 fs for 2 ns. A Hose/Hoover thermostat is utilized to maintain the temperature of the liquid film and the solid surfaces during the equilibration. Then the water and hexane system is equilibrated in an NVE ensemble. Pt_{up} and Pt_{down} are equilibrated in an NVT ensemble at 550 K and 300 K, respectively. The condensation process is simulated and data are collected at interval of 1 ns.

3. Results and discussion

3.1. Wetting of sessile droplets

Prior to investigating the dynamics of droplets, their static states on the patterned surface without lubricant are analyzed first, which is fundamental physics. The results are depicted in Fig. 3a and 3b. We can see two wetting state modes, the Cassie state with air-pocket formed between liquid and solid, and the Wenzel state with liquid fully sunk into gaps between solid surfaces. These two wetting states can be determined by the energy parameter $\varepsilon_{W\text{-}Pt}$: the droplet in the Cassie state here corresponds to $\varepsilon_{W\text{-}Pt}$ = 0.01 eV while the other one in the Wenzel state corresponds to $\varepsilon_{W\text{-}Pt}$ = 0.02 eV.

As shown in Fig. 3c, three types of interfaces can be observed when the same structure is impregnated with lubricants, including the water–vapor-lubricant, solid-water-lubricant, and solid–vapor-lubricant interfaces. Our previous work [37] found that eight types of these interfaces can form for nanodroplets on lubricant-impregnated surfaces. And three modes can be observed including the non-cloaking state, encapsulated, and encapsulated-rough states. However, in the present work, only the droplet in the slippery Wenzel state on the lubricant-impregnated wedge-groove surface is applied, as it is typical and able to elucidate the basics of our target question.

3.2. Self-driven transport

To investigate the effect of surface structures, the dynamics of existing droplets are examined on two types of surface structure: parallel-grooves and wedge-grooves. The droplets on wedge-grooves can present two wetting status, here named as wedge-groove Cassie and wedge-groove Wenzel. In addition, the wedge-groove with lubricant can lead to a special wetting status, named as wedge-groove LIS. Totally, four types of wetting modes are used

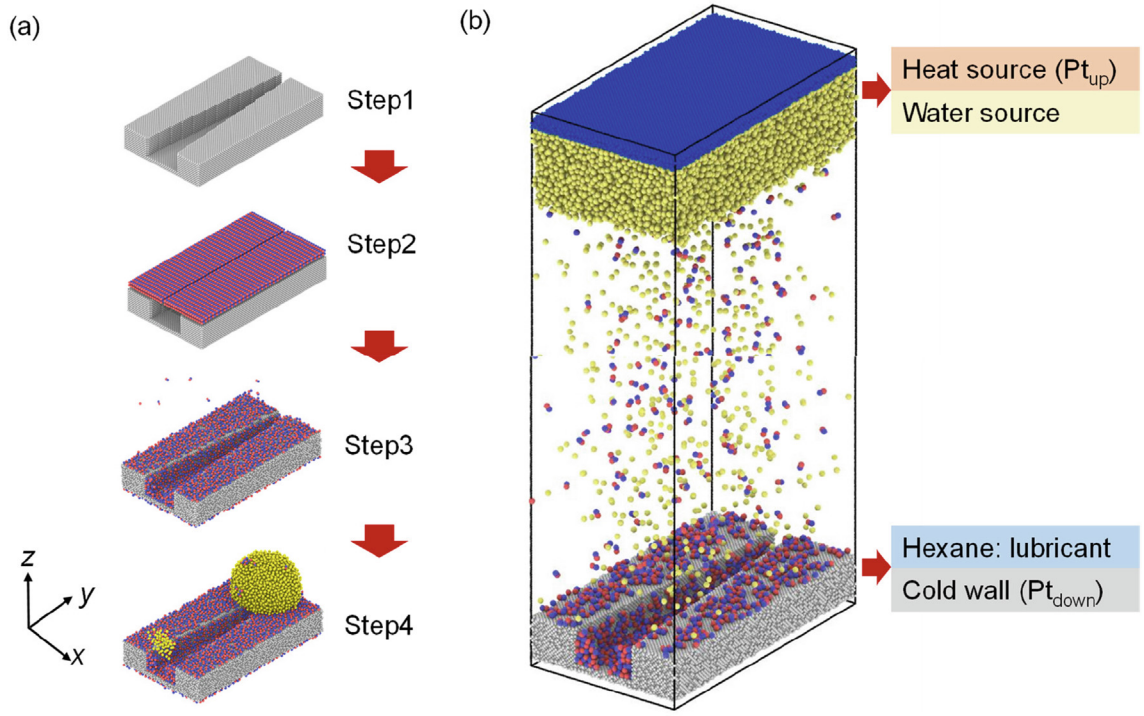

Fig. 2. Simulation procedures. (a) Simulation of the single droplet dynamics on patterned surfaces. Step 1: the wedge-groove structure is built as the substrate; Step 2: the hexane beads are placed on top of the substrate; Step 3: the whole system is equilibrated at 300 K using a Nose/Hoover thermostat with a time step of 10 fs for 1 ns; Step 4: the whole system is equilibrated in an NVE ensemble and runs for 10 ns with a time step of 10 fs. (b) Condensation simulation configurations. The liquid film at the top of the simulation box is used as a vapor source, and the solid surface on top of the film is treated as the heat source (Pt_{up}). The solid surface on the bottom of the simulation box is treated as the surface for condensation (Pt_{down}) with lubricant on top of it.

Table 2
Surface geometry parameters.

Parameters	Parallel-groove	Wedge-groove	Wedge-groove LIS
Conical angle α / °	0	9.5	9.5
Groove length L / Å	274.4	274.4	274.4
Spacing s / Å	31.36	16.98	24.82
Groove depth h / Å	15.68	15.68	23.52

and the dynamics of droplets are summarized in Fig. 4. The wedge-groove Cassie (see Fig. 4b) refers to the case for which the droplet is in the Cassie state while the wedge-groove Wenzel (see Fig. 4c) refers to the case for which the droplet is in the Wenzel state on the wedge-groove substrate.

Note firstly that droplets remain static on the parallel-groove and wedge-groove Cassie surfaces (see Fig. 4a and b). In contrast, a spontaneous movement is observed for the droplets of wedge-groove Wenzel and wedge-groove LIS, from the narrower side to the wider side (see Fig. 4c and d). The droplet dynamic characters are described by the average velocity, which is plotted in Fig. 4e. The velocity of the self-driven droplet on the wedge-groove LIS reaches 5.28 m/s, which is twice that of the wedge-groove Wenzel, indicating a large potential in driving droplets on the proposed structure.

To decipher the underlying principle of the different droplet dynamics, a theoretical analysis is conducted for a droplet placed on the wedge-groove surface, as shown in Fig. 5. The droplet is in the Wenzel state on the wedge-groove surface, so the bottom of the droplet can completely wet the conical groove walls; a three-dimensional shape is shown in red in Fig. 5a. The spacing of the conical groove changes along the y-direction, leading to a gradient of the base radius and thus a Laplace pressure difference. A component F_{iy} in the y-direction is formed because of the unbalanced interface tensions, as shown in Fig. 5b. The driving force is

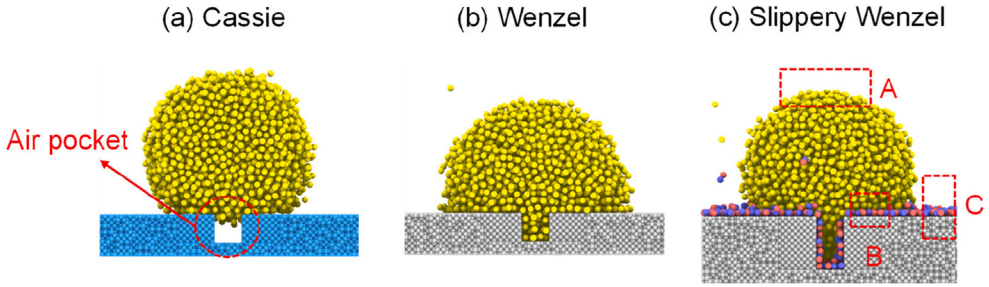

Fig. 3. Static states. The surface wetting state can be controlled by the energy parameter. The droplet is in (a) the Cassie state when $\varepsilon_{W\text{-}Pt}$ = 0.01 eV (distinguished by the blue color) and in (b) the Wenzel state when $\varepsilon_{W\text{-}Pt}$ = 0.02 eV. (c) There are three interfaces for a droplet on a lubricantimpregnated surface: water–vapor-lubricant (A), solid-water-lubricant (B), and solid-vapor-lubricant (C). By using parameters in Table 1, these three interfaces are in the non-cloaking, encapsulated, and encapsulated-rough states, respectively. The droplet is in the slippery Wenzel state.

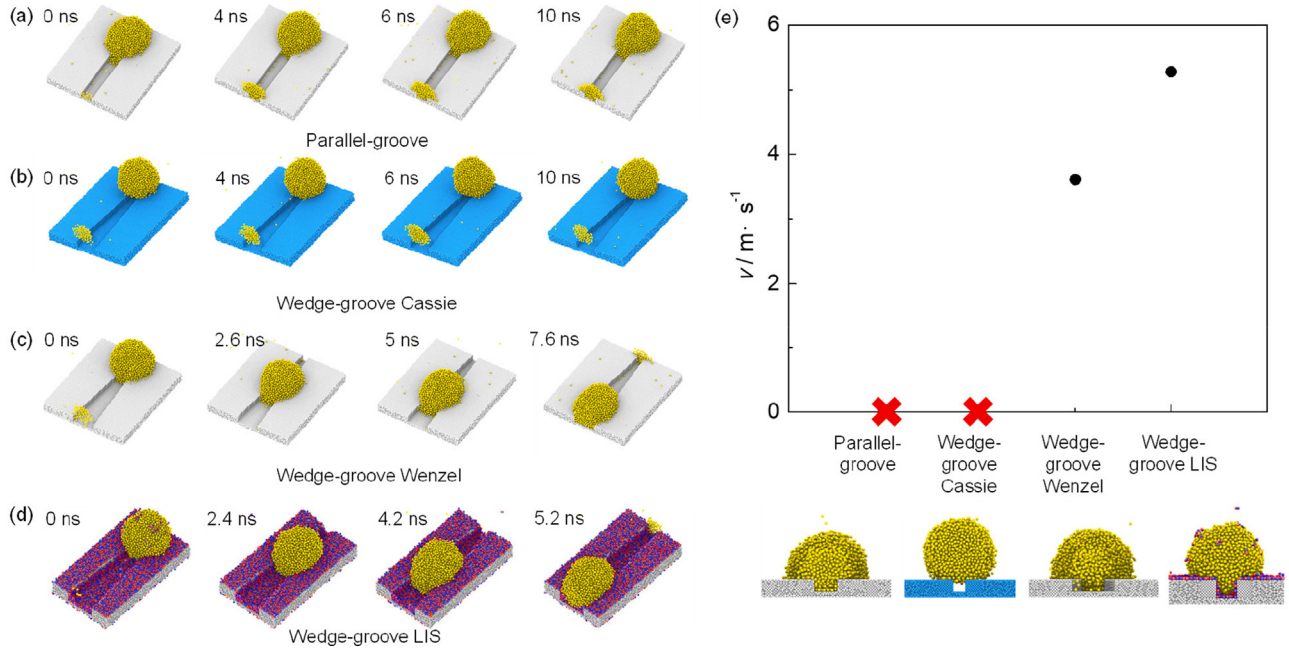

Fig. 4. Time-lapsed images of droplet moving process on (a) parallel-groove surface, (b) wedge-groove Cassie surface, (c) wedge-groove Wenzel surface, and (d) wedge-groove LIS surface. (e) The average velocity v of different surfaces. Droplets that cannot move are marked by red cross.

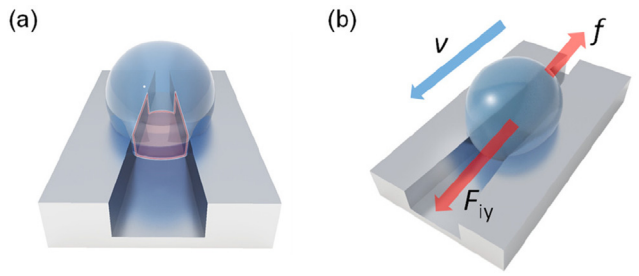

Fig. 5. Theoretical analysis of droplet self-driven behavior. (a) The interface squeezed by the wedge groove; (b) Force analysis for a droplet on the wedge groove. F_{iy} refers to component in the y-coordinate of the driving force. f refers to frictional force during droplet movement.

able to overcome the frictional force f generated against the direction of movement, which eventually drives the droplet to move on the wedge-groove substrate. Moreover, the frictional force is decreased by the lubricant on the wedge-groove LIS because the liquid–solid interface is replaced by the solid-water-lubricant interface. There is no driving force formed on the parallel-groove because the spacing of the groove keeps unchanged. So, the droplet keeps still on the parallel-groove surface. A liquid–vapor interface is formed at the bottom of the Cassie droplet due to the air pocket. Despite the conical shape, the driving force generated by the uneven interface tension is not large enough to overcome the friction force and move the droplet. It is interesting to note that the "sticky" Wenzel droplet can move spontaneously while the "sliding" Cassie state remains still on wedge-groove surfaces. This phenomenon is of great potential for condensate manipulation and heat transfer enhancement during condensation on the wedge-groove structure.

3.3. Self-propulsion dependence on surface

The self-driven transport on the wedge-groove LIS exhibits great potential of manipulating droplets without external energy and enriches the detachment strategy of condensates. There are three parameters determining the structure of the wedge-groove LIS: the conical angle, the groove depth, and the lubricant thickness. In addition, the interaction force between water and substrates also affects the droplet movement. Therefore, the effects of these parameters on the droplets dynamic behaviours are explored and the optimizations are conducted in this section.

(1) Effect of conical angle

The self-driven process and velocity of droplets under different conical angles are shown in Fig. 6. When the conical angle is as small as 3.3°, the gradient of base radius is not large enough and the driving force is not sufficient to move the droplet. The droplet starts to move and the velocity increases as the conical angle increases. However, when the conical angle is too large (α = 16.0°), the droplet can only move halfway and then sink into the groove. The driving force is not large enough to overcome the increased frictional force. Therefore, it is necessary to consider the combined effect of conical angle on the driving force and the frictional force.

(2) Effect of the groove depth

Fig. 7 shows the effects of the groove depth on the droplet movement. It can be observed that the droplet can move directionally with a velocity of 4.3 m/s when the depth of the groove is only 7.84 Å. The droplet velocity increases as the depth of the groove increases to 31.36 Å. But the droplet is observed immobile when the depth increases to 54.88 Å. The reason is that the droplet can completely wet the groove when the depth is small and stays in the slippery Wenzel state. An air pocket is formed when the depth is higher than 31.36 Å. The slippery Wenzel state is transferred to the unexpected slippery Cassie state, as shown in Fig. 7b. The groove depth should not be too large to avoid the formation of the Cassie state.

(3) Effect of the lubricant thickness

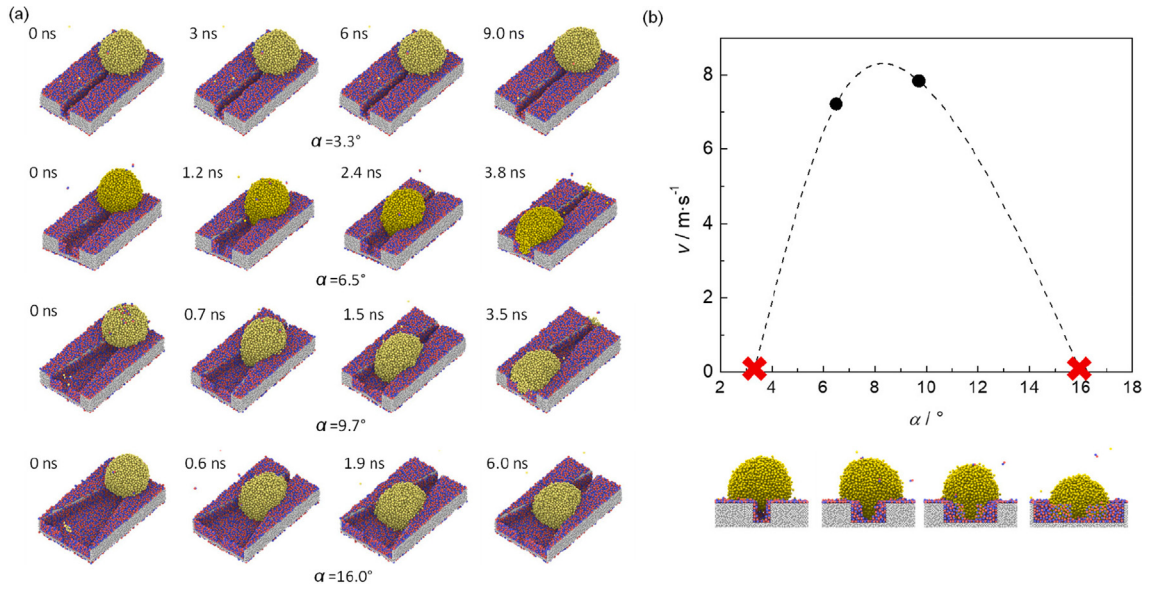

Fig. 6. Effects of the conical angle on the droplet self-driven movement. (a) Time-lapsed images and (b) average velocities under different conical angles α. Droplets that cannot move are marked by red cross.

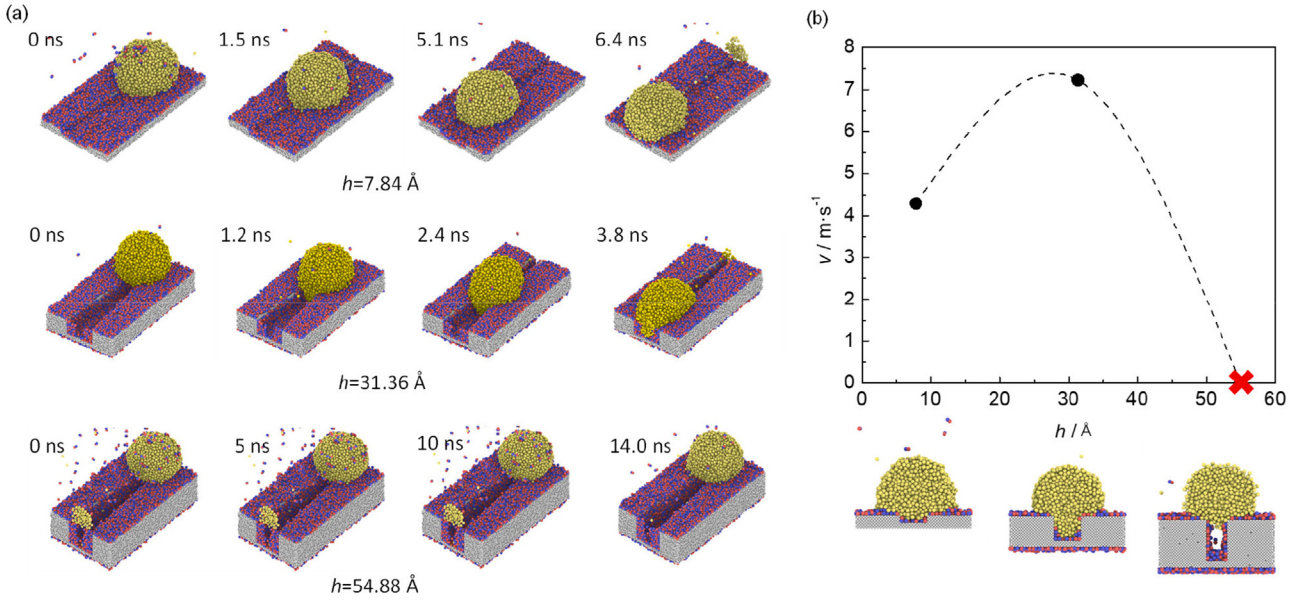

Fig. 7. Effects of the groove depth on the droplet self-driven movement. (a) Time-lapsed images and (b) average velocities under different groove *h*. Droplet that cannot move is marked by red cross.

The effect of the lubricant thickness on the droplet dynamic behaviour is investigated. Fig. 8 shows the droplet moving processes and corresponding velocities under different hexane numbers of *N*. It can be seen from Fig. 8(a) that the droplet can move spontaneously at various lubricant thicknesses, but with different speeds. The velocity of the droplet increases at first as the lubricant thickness increases, as shown in Fig. 8(b). When the hexane number increases to 2244, the lubricant can completely cover the solid wedge-groove. The friction force decreases significantly due to the fully replaced liquid–solid interface, resulting in a faster movement of the droplet. However, as the lubricant thickness keeps on increasing, the driving force decreases due to the reduced groove height as a consequence of the increased lubricant thickness. Furthermore, the friction force is enlarged by the over-thick lubricant. The droplet velocity begins to decrease as a result. When the thickness of lubricant increases appropriately, it could be beneficial for the droplet movement. When the thickness of lubricant is too large, it will hinder droplet movement instead. The lubricant should be carefully impregnated to reach the best performance.

(4) Effect of the water-substrate interaction

The interaction force between water and substrates is controlled by the energy parameter $\varepsilon_{W\text{-}Pt}$. Therefore, droplet dynamic behaviours under different $\varepsilon_{W\text{-}Pt}$ are studied and shown in Fig. 9. Note firstly that the droplet will not move when $\varepsilon_{W\text{-}Pt}$ = 0.015 eV. The reason is that the droplet would be in Cassie state if the energy parameter was too small. With the increase of $\varepsilon_{W\text{-}Pt}$, droplets can form Wenzel state and move spontaneously to the wider side of the groove. The velocity increases first but decreases as the energy

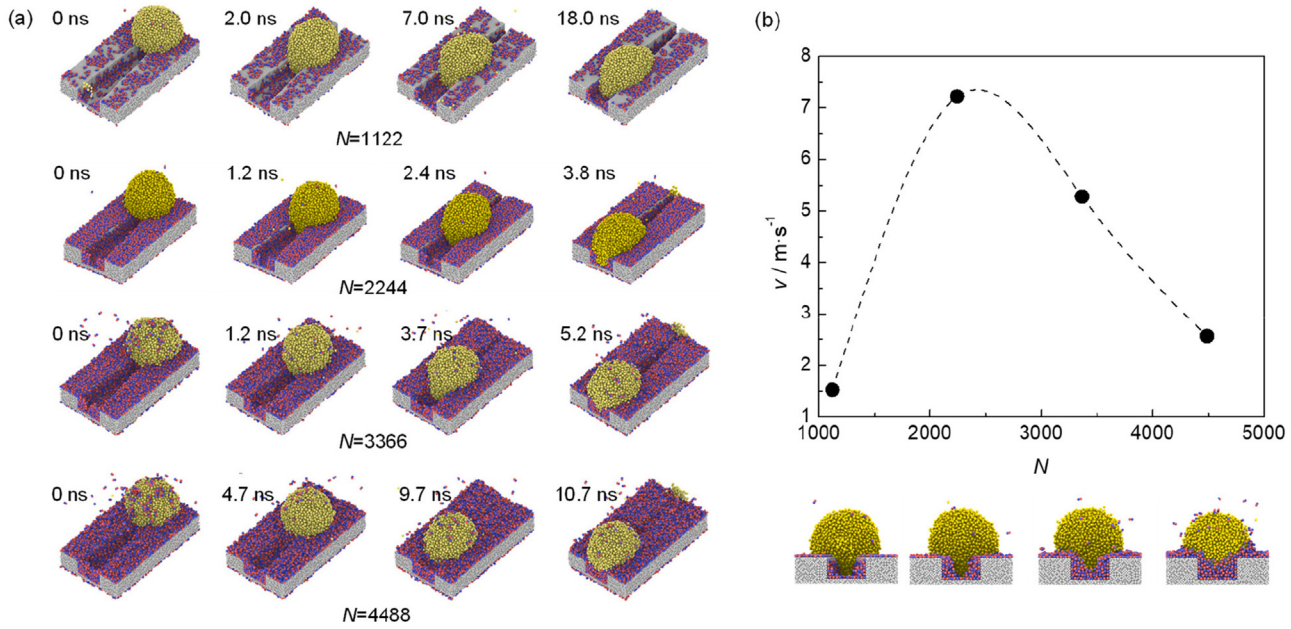

Fig. 8. Effects of the lubricant thickness on the droplet self-driven movement. (a) Time-lapsed images and (b) average velocities under different hexane numbers *N*.

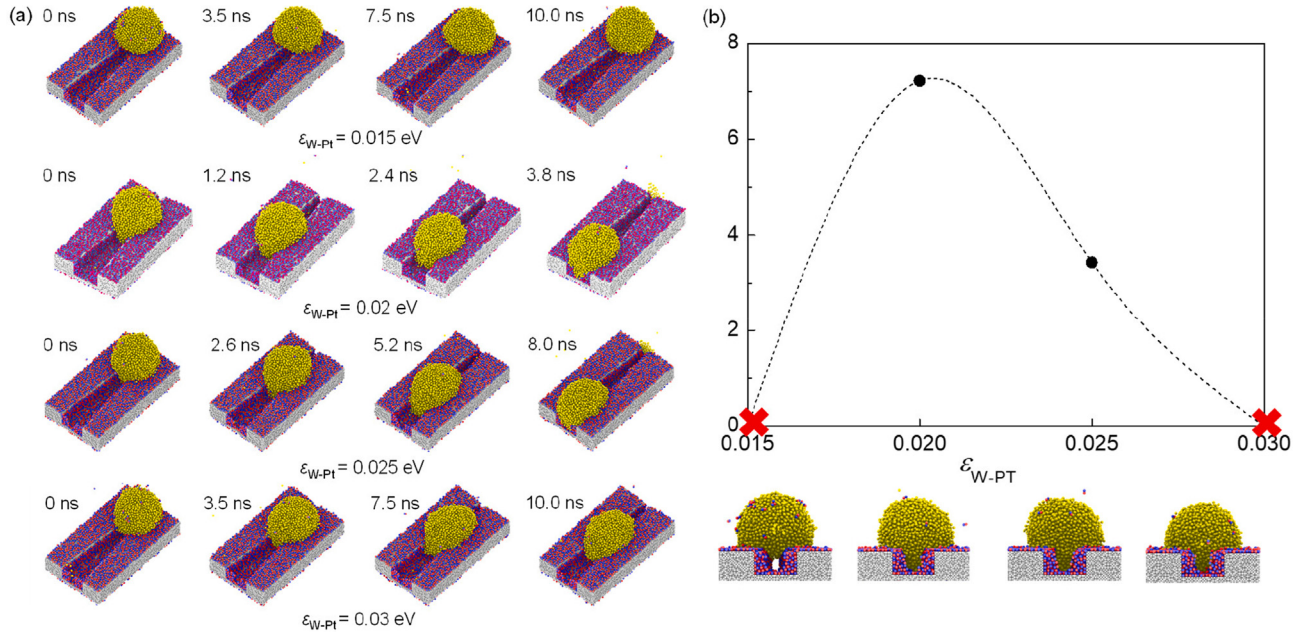

Fig. 9. Effects of the energy parameter $\varepsilon_{W\text{-}Pt}$ on the droplet self-driven movement. (a) Time-lapsed images and (b) average velocities.

parameter keeps enlarging, and fails to move when $\varepsilon_{W\text{-}Pt}$ reaches 0.03 eV. The increased $\varepsilon_{W\text{-}Pt}$ enlarges the interaction force between water and substrate, which leads to a larger moving resistance during droplet motion.

3.4. Coupling of condensation and propulsion

Above the dynamics of an existing nanodroplet are examined, and now we turn to investigate the dynamics of condensing droplets. To understand the effects of lubricant, a set of simulations are performed for comparisons, including five cases of the wedge-groove LIS surface, normal smooth surface, parallel-groove surface and two types of wedge-groove surfaces with different wettability. Time-lapsed snapshots during condensations are collected and shown in Fig. 10. Vapor nucleation and cluster formation are observed on all the cases, expect for Case C. It can be observed first that no cluster is formed on the wedge-groove Cassie surface (see Fig. 10c), which is attributed to the higher energy barrier for nucleation on a hydrophobic surface and thus a lower nucleation rate. The nanodroplets can form and continue to grow by condensation and/or coalescence with other nanodroplets. Fig. 11a presented the time evolutions of the molecular number in condensate, where only a slight difference can be observed among the cases of the smooth, the parallel-groove, and the wedge-groove Wenzel. Correspondingly, the condensation rates are shown in Fig. 11b. The details are discussed as below.

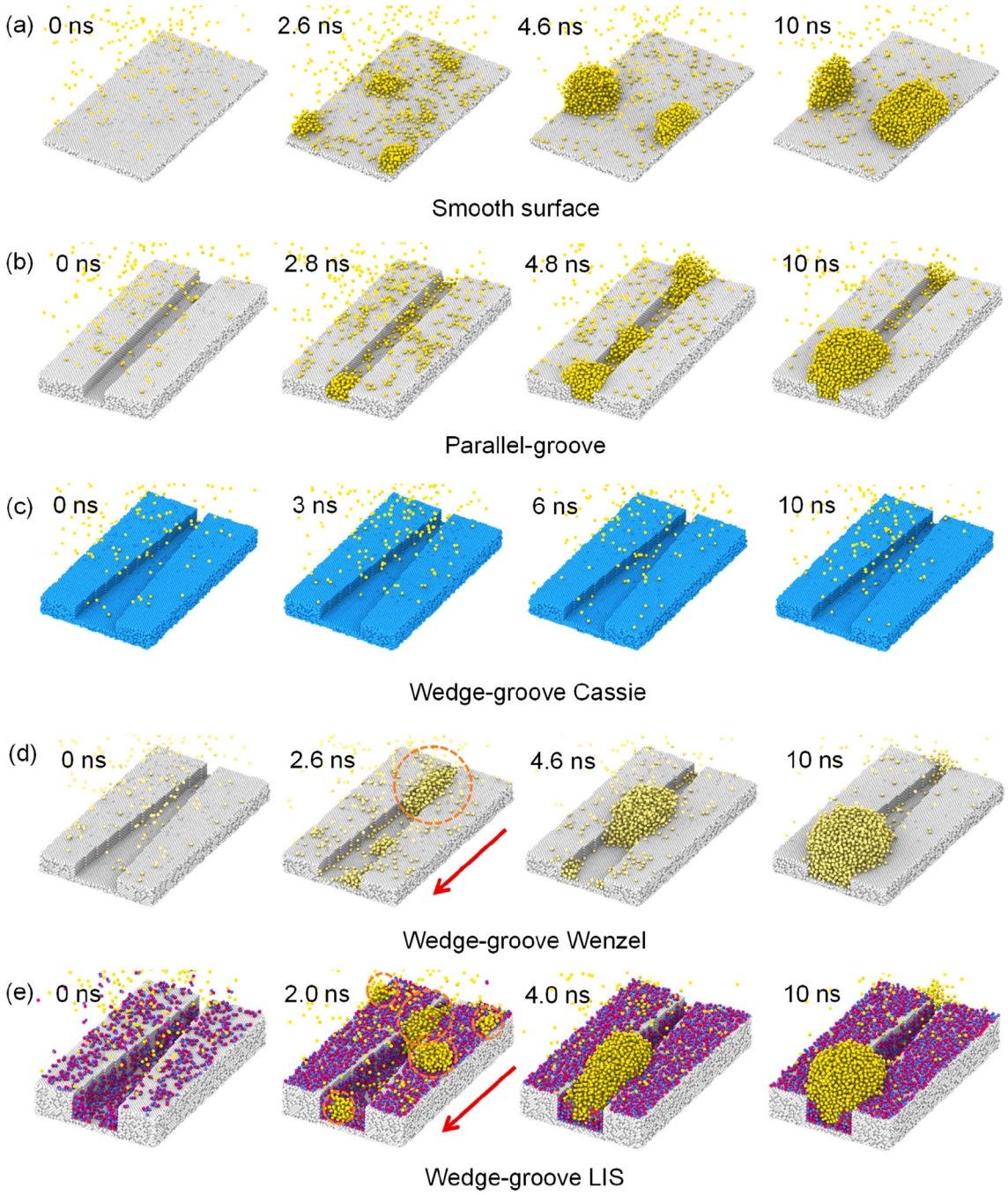

Fig. 10. Time-lapsed images during condensation on surfaces with different patterns. Clusters prefer to form at the narrow side of the wedge groove and are marked with dashed circles in case d. More clusters are found on case marked with dashed circles. Clusters in wedge grooves can move in the direction indicated by the arrow.

(1) Nucleation site

A random and discrete cluster formation is observed on the smooth surface, as shown in Fig. 10a. At t = 2.6 ns, four nuclei are seen although their shape is not strictly hemispherical, and then they merge with each other, leading to a roughly stable contact angle until t = 10 ns. Additionally, it is found that no wondering is observed for these nanodroplets unless a coalescence occurs. This is different from the vapour nucleation on super-hydrophobic surfaces, where initially-formed nanodroplets can present nucleation-induced wondering randomly [42]. Even though the wettability of the present smooth surface is not measured, its hydrophilicity can be inferred according to not only the snapshot in Fig. 10a, but also the contact angle of a droplet in Wenzel mode (see Fig. 3). The uncontrolled and immobile nucleation here is not preferred as it means a small potential for sliding or shedding off.

On the location of nucleation, as shown in Fig. 10b and 10d, the grooves show the potential of controlling the nucleation site. Clusters prefer to form in the grooves other than the top parts. The clusters are randomly formed in the parallel groove, see Fig. 10b. Water molecules condense continuously with time going on. Three clusters are found in the parallel groove and then merge into a large one. As for surfaces with wedge groove, water clusters prefer to form at the narrow side of the wedge groove at first, see Fig. 10d. For a condensation process, the nucleation free energy barrier ΔG_r for a cluster derived by Liu and Cheng can be expressed as [43]

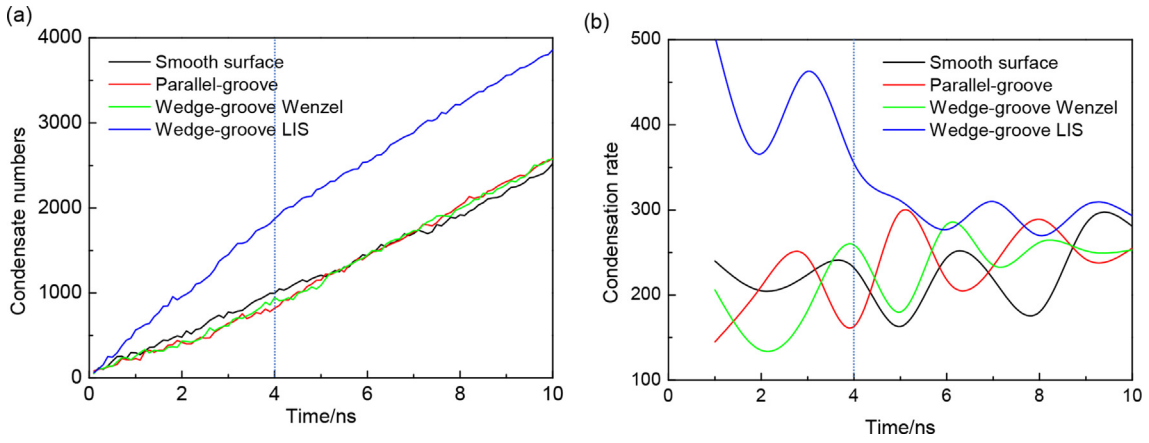

Fig. 11. (a) Condensate water numbers along with time; (b) Condensation rate.

$$\Delta G_r = \rho_c \int \frac{H_{fg}(T_l(r,\varphi) - T_s)}{T_{sat}} dV + \sigma_{lv}(2 - 3\cos\theta + \cos^3\theta)\pi r^2. \quad (4)$$

For a cluster formed on a surface with grooves, the cluster volume on a narrower groove will be smaller than that on a wider groove. The radius of clusters on the narrower groove is accordingly smaller. As a result, the cluster on the narrower groove has a smaller nucleation free energy barrier based on Eq. (4). Moreover, with the constrains of the narrow space, the cluster is more stable, which is in favor of the following nucleating and growing process. As shown in Fig. 10e, with the introduction of lubricant, t = 2.0 ns four discrete nuclei are observed near the groove while one is found within the narrow side, which presents the highest nucleation rate among these cases. Moreover, the contact angles of these initially-formed nuclei are slightly larger those on the smooth surface. Thus, the wetting of initial nuclei is consistent with that of stable nanodroplets as shown in Fig. 3. Furthermore, it should be noted that the condensation rate is different from the nucleation rate, which will be discussed in the next section.

(2) Condensation rate

Although the noticeable differences are observed in nucleation sites, it is interesting to see small differences in condensation rate among the three cases in Fig. 10a, b, d. In contrast, the wedge-groove LIS surface has the largest condensation number, indicating a larger nucleation rate. The reason is that the energy barrier of condensation is primarily reduced by the lubricant by replacing the liquid–solid interface with the water-lubricant-solid interface. The condensation rate of the wedge-groove LIS is larger than the other three cases at the beginning of the condensation, but decreases after 4 ns and becomes almost the same as the other three cases, see Fig. 11b. Discrete clusters merge to one large cluster at 4 ns. Then the vapor prefers to condense on the cluster surface instead of the substrate, leading to a decreased condensation rate.

(3) Condensing and self-driving

Instead of the immobile condensing droplets, an interaction between condensing and self-driving is observed on the surfaces of wedge-groove Wenzel and wedge-groove LIS due to the Laplace pressure difference. In details, clusters on the top side merge with the cluster in the groove and move directionally towards the wider side with the action of the wedge-shaped groove. After coalescences, one large nanoscale droplet is observed. This droplet continues growing up by collecting condensing water molecules.

The wedge-groove LIS structure can not only control the nucleation site but also present a high efficiency in self-driving of condensing droplets. In details, it takes about 7 ns for the merged cluster to reach the wide side on the wedge-groove Wenzel surface, while it takes only 4 ns on the wedge-groove LIS surface. Moreover, the high efficiency can deserve more credits considering that the size of the final droplet is almost one time larger than that on the wedge-groove Wenzel surface.

3.5. Discussion

It is still necessary to contextualize the impacts of the results above, rather than just present interesting but independent MD simulation results. A discussion is briefly conducted on the connection between the present work and relevant experimental work. In the work by Guo and Tang in 2018, a copper-based hydrophilic-slippery surface to explore a possibility of both enhanced nucleation rates and efficient droplet sliding [39]. A stable dropwise condensation is realized on a hydrophilic surface, which was confirmed by an experimental work by Cha et al. in 2020 [44]. The ground-breaking effects of these advances encourage more exploration along this direction.

The present work may provide some response on the nucleation rate, droplet mobility and overall condensation rate, each of which will be given with an example. On the nucleation, as shown in Fig. 8 in Ref. [37], it takes about 16 s and 7 s for droplets to be observed on superhydrophobic (SHPO) and hydrophobic (HPO) surfaces, respectively. However, on two types of lubricant-impregnated surface, it just takes less than 1 s for droplets to nucleate and increase up to sufficient size to be visible. On the mobility, it was experimentally found that nucleation is facilitated on the hydrophilic untreated copper surface, but the micro-droplet strongly pins on the surface. This is consistent with the present simulation results for nanodroplets on smooth surface (see Fig. 10a). In the experimental work, lubricant-impregnated surfaces present an enhanced condensation rate, as shown by the enhanced surface coverage, droplet density and heat transfer performance. Correspondingly, an enhancement in the number of molecules in condensation is also observed as shown in Fig. 11a. Overall, although the present results are obtained by MD simulation at nanoscale, it is still helpful and meaningful to provide the details of underlying physics, which are invisible for experimental measurement and observation, and are also supplementary information of macroscopic process.

4. Conclusions.

In summary, a bionic lubricant-impregnated wedge-groove surface is proposed in present work to manipulate condensates in the Wenzel state. The self-driven transport of a single nanodroplet and condensate is achieved using the molecular dynamics simulation. The effects of the wetting states, lubricant thickness, groove depth and cone angle on droplet dynamic characteristics are systematically studied. The results show that the proposed surface can drive droplets in the Wenzel state to move spontaneously by taking advantage of the wedge shape and the thoroughly wetted liquid–solid interface in the groove. The nucleation site is also observed to be controlled by the wedge-groove structure. In addition, the impregnated lubricant can reduce the frictional force as well as the energy barriers of nucleation. By manipulating condensates in the Wenzel state, both the nucleation rate and the refresh rate of condensed surfaces are improved, which can expand the application range of the subcooling degree and the surface durability. We envision that the present work enriches the strategy of condensate manipulations and enhancement of condensation heat transfer.

Funding resources

This work was financially supported by the National Natural Science Foundation of China through contract Nos. 51825604 and 52076113, and the Natural Science Foundation of Shandong Academy of Sciences through contract Nos. 2019No.2 and 2020KJC-GH04, and the Shandong Provincial Key Research and Development Program through contract No. 2019GGX103031.

CRediT authorship contribution statement

Lin Guo: Investigation, Writing – original draft. **Wenqing Shen:** Validation, Writing – review & editing. **Kumar Satish:** Validation, Writing – review & editing. **Zhigang Liu:** Supervision, Project administration, Writing – review & editing. **Guihua Tang:** Supervision, Project administration, Writing – review & editing.

Declaration of Competing Interest

The authors declare that they have no known competing financial interests or personal relationships that could have appeared to influence the work reported in this paper.

References

[1] T.Y. Zhang, L.W. Mou, J.Y. Zhang, L.W. Fan, J.Q. Li, A Visualized Study of Enhanced Steam Condensation Heat Transfer on a Honeycomb-Like Microporous Superhydrophobic Surface in the Presence of a Non-Condensable Gas, Int. J. Heat Mass Transf. 150 (2020) 119352.
[2] J. Xie, Q.T. She, J.L. Xu, C. Liang, W.X. Li, Mixed Dropwise-Filmwise Condensation Heat Transfer on Biphilic Surface, Int. J. Heat Mass Transf. 150 (2020) 119273.
[3] R. Wang, F.F. Wu, D.D. Xing, X.F. Gao, Density Maximization of One-Step Electrodeposited Copper Nanocones and Dropwise Condensation Heat-Transfer Performance Evaluation, ACS Appl. Mater. Interfaces 12 (21) (2020) 24512–24520.
[4] G.H. Tang, H.W. Hu, D. Niu, L. Guo, Q. Sheng, Y. Shi, Advances in Vapor Dropwise Condensation Heat Transfer, Chin. Sci. Bull. 65 (17) (2020) 1653–1676.
[5] I. Oh, H. Cha, J.H. Chen, S. Chavan, H. Kong, N. Miljkovic, Y.H. Hu, Enhanced Condensation on Liquid-Infused Nanoporous Surfaces by Vibration-Assisted Droplet Sweeping, ACS Nano 14 (10) (2020) 13367–13379.
[6] M.S. Alam, J.H. Jeong, Molecular Dynamics Simulations on Homogeneous Condensation of R600a Refrigerant, J. Mol. Liq. 261 (2018) 492–502.
[7] J.C. Ma, S. Sett, H. Cha, X. Yan, N. Miljkovic, Recent Developments, Challenges, and Pathways to Stable Dropwise Condensation: A Perspective, Appl. Phys. Lett. 116 (26) (2020) 260501.
[8] M.V. Ushcats, L.A. Bulavin, V.M. Sysoev, V.Y. Bardik, A.N. Alekseev, Statistical Theory of Condensation - Advances and Challenges, J. Mol. Liq. 224 (2016) 694–712.
[9] Q. Xue, Z. Lan, W. Li, F. Chen, R. Wen, X. Ma, Z. Zhao, Detection and Experimental Analysis of the Molecular Clusters Distribution During Wall Condensation, J. Mol. Liq. 116948 (2021).
[10] D. Quere, Wetting and Roughness, Annu. Rev. Mater. Res. (2008) 71–99.
[11] S. Baba, K. Sawada, K. Tanaka, A. Okamoto, Dropwise Condensation on a Hierarchical Nanopillar Structured Surface, Langmuir 36 (34) (2020) 10033–10042.
[12] M. Hekmatifar, D. Toghraie, B. Mehmandoust, F. Aghadavoudi, S. Ali Eftekhari, Molecular Dynamics Simulation of Condensation Phenomenon of Nanofluid on Different Roughness Surfaces in the Presence of Hydrophilic and Hydrophobic Structures, J. Mol. Liq. 334 (2021).
[13] K. Hosseinzadeh, D.D. Ganji, F. Ommi, Effect of SiO2 Super-Hydrophobic Coating and Self-rewetting Fluid on Two Phase Closed Thermosyphon Heat Transfer Characteristics: An Experimental and Numerical Study, J. Mol. Liq. 315 (2020).
[14] K.L. Wilke, D.J. Preston, Z.M. Lu, E.N. Wang, Toward Condensation-Resistant Omniphobic Surfaces, ACS Nano 12 (11) (2018) 11013–11021.
[15] T. Foulkes, J. Oh, P. Sokalski, L.N. Li, S. Sett, J. Sotelo, X. Yan, R. Pilawa-Podgurski, A. Castaneda, M. Steinlauf, N. Miljkovic, Jumping Droplets Electronics Cooling: Promise versus Reality, Appl. Phys. Lett. 116 (20) (2020) 203701.
[16] R.F. Wen, S.S. Xu, X.H. Ma, Y.C. Lee, R.G. Yang, Three-Dimensional Superhydrophobic Nanowire Networks for Enhancing Condensation Heat Transfer, Joule 2 (2018) 269–279.
[17] R.F. Wen, Z. Lan, B.L. Peng, W. Xu, X.H. Ma, Wetting Transition of Condensed Droplets on Nanostructured Superhydrophobic Surfaces: Coordination of Surface Properties and Condensing Conditions, ACS Appl. Mater. Interfaces 9 (15) (2017) 13770–13777.
[18] X. Yan, F. Chen, S. Sett, S. Chavan, H. Li, L. Feng, L. Li, F. Zhao, C. Zhao, Z. Huang, N. Miljkovic, Hierarchical Condensation, ACS Nano 13 (7) (2019) 8169–8184.
[19] W. Ding, M. Wang, X. Dai, J. Zhang, G. Xin, X. Wang, Dewetting Transition of Water on Nanostructured and Wettability Patterned Surfaces: A Molecular Dynamics Study, J. Mol. Liq. 336 (2021).
[20] N. Miljkovic, R. Enright, Y. Nam, K. Lopez, N. Dou, J. Sack, E.N. Wang, Jumping-Droplet-Enhanced Condensation on Scalable Superhydrophobic Nanostructured Surfaces, Nano Lett. 13 (1) (2013) 179–187.
[21] N. Miljkovic, D.J. Preston, R. Enright, E.N. Wang, Electrostatic Charging of Jumping Droplets, Nature Communacation 4 (2013) 2517.
[22] D.D. Xing, R. Wang, F.F. Wu, X.F. Gao, Confined Growth and Controlled Coalescence/Self-Removal of Condensate Microdrops on a Spatially Heterogeneously Patterned Superhydrophilic-Superhydrophobic Surface, ACS Appl. Mater. Interfaces 12 (26) (2020) 29946–29952.
[23] J.H. Pu, S.K. Wang, J. Sun, W. Wang, H.S. Wang, Growth and Self-jumping of Single Condensed Droplet on Nanostructured Surfaces: A Molecular Dynamics Simulation, J. Mol. Liq. 116902 (2021).
[24] B. El Fil, G. Kini, S. Garimella, A Review of Dropwise Condensation: Theory, Modeling, Experiments, and Applications, Int. J. Heat Mass Transf. 160 (2020) 120172.
[25] X.M. Dai, N. Sun, S.O. Nielsen, B.B. Stogin, J. Wang, S.K. Yang, T.S. Wong, Hydrophilic Directional Slippery Rough Surfaces for Water Harvesting, Science, Advances 4 (3) (2018) eaaq0919.
[26] S.L. Huang, J. Li, L. Liu, L.D. Zhou, X.L. Tian, Lossless Fast Drop Self-Transport on Anisotropic Omniphobic Surfaces: Origin and Elimination of Microscopic Liquid Residue, Adv. Mater. 1901417 (2019).
[27] J. Sun, P. Weisensee, Microdroplet Self-Propulsion During Dropwise Condensation on Lubricant-Infused Surfaces, Soft Matter 15 (2019) 4808–4817.
[28] X. Tang, H. Xiong, T. Kong, Y. Tian, W.-D. Li, L. Wang, Bioinspired Nanostructured Surfaces for On-Demand Bubble Transportation, ACS Appl. Mater. Interfaces 10 (3) (2018) 3029–3038.
[29] G.K. Sirohia, X.M. Dai, Designing Air-Independent Slippery Rough Surfaces for Condensation, Int. J. Heat Mass Transf. 140 (2019) 777–785.
[30] A. Goswami, S.C. Pillai, G. McGranaghan, Surface Modifications to Enhance Dropwise Condensation, Surf. Interfaces 25 (2021) 101143.
[31] Y.H. Sun, Z.G. Guo, Recent Advances of Bioinspired Functional Materials with Specific Wettability: From Nature and beyond Nature, Nanoscale Horiz. 4 (1) (2019) 52–76.
[32] M.M. Cui, B. Wang, Z.K. Wang, Nature-Inspired Strategy for Anticorrosion, Adv. Eng. Mater. 21 (7) (2019) 1801379.
[33] J. Ju, H. Bai, Y. Zheng, T. Zhao, R. Fang, L. Jiang, A Multi-Structural and Multi-Functional Integrated Fog Collection System in Cactus, Nature Communacation 3 (2012) 1247.
[34] L. Guo, G.H. Tang, Experimental Study on Directional Motion of a Single Droplet on Cactus Spines, Int. J. Heat Mass Transf. 84 (2015) 198–202.
[35] T.S. Wong, S.H. Kang, S.K.Y. Tang, E.J. Smythe, B.D. Hatton, Bioinspired Self-Repairing Slippery Surfaces with Pressure-Stable Omniphobicity, Nature 477 (7365) (2011) 443–447.
[36] H.W. Chen, P.F. Zhang, L.W. Zhang, H.L. Liu, Y. Jiang, D.Y. Zhang, Z.W. Han, L. Jiang, Continuous Directional Water Transport on the Peristome Surface of Nepenthes alata, Nature 532 (7597) (2016) 85–89.
[37] L. Guo, G.H. Tang, S. Kumar, Droplet Morphology and Mobility on Lubricant-Impregnated Surfaces: A Molecular Dynamics Study, Langmuir 35 (49) (2019) 16377–16387.

[38] J.D. Smith, R. Dhiman, S. Anand, E. Reza-Garduno, Droplet mobility on lubricant-impregnated surfaces, Soft Matter 9 (6) (2013) 1772–1780.
[39] L. Guo, G.H. Tang, Dropwise Condensation on Bioinspired Hydrophilic-Slippery Surface, RSC Adv. 8 (69) (2018) 39341–39351.
[40] X. Dai, B.B. Stogin, S. Yang, T.S. Wong, Slippery Wenzel State, ACS Nano 9 (9) (2015) 9260–9267.
[41] L. Guo, G.H. Tang, S. Kumar, Dynamic Wettability on the Lubricant-Impregnated Surface: From Nucleation to Growth and Coalescence, ACS Appl. Mater. Interfaces 12 (23) (2020) 26555–26565.
[42] Q. Sheng, J. Sun, Q. Wang, W. Wang, H.S. Wang, On the Onset of Surface Condensation: Formation and Transition Mechanisms of Condensation Mode, Sci. Rep. 6 (2016) 30764.
[43] X. Liu, P. Cheng, Dropwise condensation theory revisited: Pare I. Droplet nucleation radius, Int. J. Heat Mass Transf. 83 (2015) 833–841.
[44] H. Cha, H. Vahabi, A. Wu, S. Chavan, M.-K. Kim, S. Sett, S.A. Bosch, W. Wang, A. K. Kota, N. Miljkovic, Dropwise Condensation on Solid Hydrophilic Surfaces, Sci. Adv. 6 (2020) eaax0746.